

Supplementary Information

Robotic soft swim bladder using liquid-vapor phase transition

*Beomchan Kang, Tailin Piao, Yongkyu Lee, Zhengbing Ding, and Wei David Wang**
Department of Mechanical Engineering, Hanyang University, Seoul 04763, South Korea.
*Corresponding author. Email: davidwang@hanyang.ac.kr, hitwangw@hotmail.com

Materials and Methods

Materials and Fabrication of the soft swim bladder

The heat-sealable TPU films with a thickness of 0.15 mm were first prepared as material for the pouch skin. The two TPU films were sealed using an impulse sealer with a sealing line thickness of 2 mm, leaving one side open for injecting fluid. Each pouch was then filled with 0.08 ml of liquid-vapor phase transition material using a needle and a syringe. After the pouch was filled, the remaining side was sealed. The properties of the engineered fluid are shown in Table S1. The copper-polyimide film with the copper layer (thickness of 18 μm) and PI layer (thickness of 15 μm) was prepared. As the first step, the composite film was etched with an etching solution into the desired circuit pattern. After etching, the heating element was cleaned using ethanol and water to remove the etchant and the dissolved copper remaining on the surface. To prepare a casting mold for creating the elastic cover, the designed mold was printed using an FDM type 3D printer (GUIDER II S, FlashForge). The Ecoflex 00-30 was then prepared (Part A: Part B = 1:1) and degassed in a vacuum chamber at room temperature. After the degassing process, the prepolymer was poured into a printed 3D mold and completely cured through a baking process at 60 °C for 4 h. Three buoyancy pouches were prepared using the fabrication methods above. The resistive circuit as flexible electrical heating elements were attached to both sides of the pouch with double-sided silicon tape, altogether comprising the buoyancy pouch set. The buoyancy pouch sets with heating elements were finally covered with an Ecoflex elastomer film of 1 mm using silicone rubber adhesive (Sil-Poxy, Smooth-On) and cured for 15 min.

Fabrication of the fish robot

The fish head and tail of this robot were designed first using computer-aided design (CAD) software NX (version 11), and then the head part and the tail mold were 3D-printed. An adjustable float was filled inside the fish head to be able to adjust the buoyancy of the fish robot. The tail was then cast with Ecoflex 00-30 with a rectangular hole at the center of the tail where the SMA-based soft actuator was placed. The SMA-based soft actuator consists of two SMA wires embedded in a polydimethylsiloxane (PDMS) matrix to allow the fishtail to achieve bidirectional bending deformation to propel the fish robot forwards. After preparing all the components, the 3D-printed head, swim bladder, sponge float, tail actuator, and tail fin were assembled to form a fish robot with the main dimensions shown in Fig. S7.

FEM simulation of the maximum deformation for each buoyancy pouch

A finite element simulation was performed using the simulation software ABAQUS (version 6.13) to predict the maximum expansion deformation of the buoyancy pouch at different widths. The internal surfaces of the pouch were assumed to be subject to uniform pressure, and the buoyancy pouch was meshed using S4R linear quadrilateral elements. The experimental data and modeling results were compared and presented in Fig. S1.

Testing buoyancy pouch

Experimental maximum deformation for each buoyancy pouch

To determine the maximum deformation of each buoyancy pouch depending on the pouch size, the buoyancy pouches were fabricated with different widths ranging from 5mm to 15mm with 1mm increment (the inset of Figure 3A). The thickness of the elastic cover and the length of the pouch was fixed at 1 mm and 30 mm, respectively. The fabricated sample was then submerged in hot water at a temperature of 60 °C. Since the temperature is well above the boiling temperature of the fluid, this enabled the pouch to reach its fully expanded state, due to the phase transition of the fluid from liquid to vapor. Later, photographs were taken to analyze the deformation of the pouches (Figure S1). The expansion distance of the pouch was calculated using Tracker video analysis software (version 5.1.5).

Determination of the elastic cover thickness

To decide on the optimal elastic cover thickness that yields the best performance, elastic covers with thicknesses of 0.5 mm, 1 mm, and 1.5 mm were fabricated and compared. A single buoyancy pouch with resistive circuits covered with elastic covers was connected to a wire that was fixed to the bottom of the container to leave the pouch floating in mid-water. All the experiments conducted in water discussed in this paper were conducted at a temperature of 21 °C, excluding the maximum deformation experiment, which was carried out in hot water. For this experiment, the corresponding heating and cooling times were recorded for different thickness values. The current applied to the resistive circuits for heat generation was fixed at 0.8 A.

Current optimization

Due to the delicate nature of the buoyancy pouch, continuous exposure at extreme temperatures resulted in accelerated pouch failure. To determine the optimal current that generates sufficient heat without damaging the pouch, a K-type thermocouple (MCP9600), wired to a microcontroller was placed inside the pouch to read the temperature data. For precise measurement, the thermocouple wire was fixed firmly in between the pouch layers using silicon rubber adhesive, which also enabled airtight sealing of the gap between the pouch layers. The internal temperature of the buoyancy pouch was measured under different currents ranging from 0.6 A to 1.0 A at 0.1 A increments. The temperature readings were processed through the MCP9600 unit and the Arduino UNO. The data was read every second for one minute to plot the Time-Temperature curve for the different currents.

Working life testing and current control strategy

The durability of the buoyancy pouch is an important measure for the swim bladder application. In this experiment, the working life of the buoyancy pouch was measured for different values of applied current

(0.6 A, 0.7 A, 0.8 A, and 0.9 A). It is noted that the experiment for 1.0 A was intentionally excluded from this set of experiments based on results from the previous experiment. The buoyancy pouch was fixed by a string to the bottom of the water inside a five-liter capacity container, and the working life was calculated from the moment of current application to the moment of pouch failure. A tabletop surveillance camera was used to record the pouch behavior while the current was continuously applied. These recordings were carefully analyzed afterward to detect the precise moment of pouch failure. The temperature change for the duration of this experiment was minimal and thereby had an insignificant influence on the results. Once the ideal current value was determined through this study, to preserve the pouch for longer, the current signal was slightly modified. Rather than applying a continuous current of 0.9 A to the resistive circuits, the current was dropped to 0.6 A after 3 s, which maintained the buoyancy pouch at 60 °C, at which the buoyancy pouch remained inflated.

Improving the working life of the buoyancy pouch

To compare the working life of the pouch depending on the thickness of the TPU film, the buoyancy pouches with different thicknesses of 0.15, 0.2, 0.3, and 0.5 mm were prepared and tested, as shown in Figure S2A. Each pouch was submerged and fixed in water and an electrical current of 0.8 A was applied to the resistive circuits for heat generation. The results show that the thickness of the film significantly affected its working life that increased linearly as the thickness of the pouch increased. The heating/cooling times for expanding and contracting the buoyancy pouch with different thicknesses of the TPU film were also calculated (Figure S2B). As the thickness of the film increases, both the heating and cooling times are increased. Hence, to achieve both a rapid heating and cooling time, the thickness of TPU of 0.15 mm was selected. Besides, repetitive heating and cooling processes were applied to the pouch to measure the working life of the pouch. Results show that the working life measured for intermittent current application with a cooling process was longer than that measured for the continuous current application (Figure S2C).

Weight loss test to examine the effects of penetration of the engineered fluid

To examine the degree of penetration of the engineered fluid through the plastic film at both liquid and vapor phases, we measured the change in weight of the fluid-containing samples over time at two different temperatures of the room temperature and 60 °C. For this test, we prepared four types of sealable plastic film (TPU, LDPE, HDPE, and PP), which is commercially used as materials for packing. A glass Petri dish filled with the engineered fluid of 0.08 ml was covered with the plastic film, and the film was then sealed to the top hole of the glass container with epoxy glue (Devcon), as shown in the inset of Figure S3. The measured results are shown in Figure S3. As for LDPE, HDPE, and PP, weight loss slightly increased over time at room temperature. However, a rapid decrease in weight was instantly observed as the experiment initiated at 60 °C. In the case of TPU, the results illustrate that the weight loss was negligible when the engineered fluid was maintained at the liquid phase at room temperature. Besides, the weight of the TPU sample above boiling point showed a steady decline over time, preserving approximately 85% of the initial weight after 4000 minutes (about 70 hours). The fluid loss through the penetration in TPU was the lowest compared to that of LDPE, HDPE, and PP since TPU has relatively low permeability coefficients amongst plastic films. For this reason, TPU was utilized as materials for buoyancy pouch covers in this study to minimize issues on weight loss.

Soft swim bladder test

Buoyancy force experiment

The fabricated soft swim bladder is detailed in Figure S4. The buoyancy force generated by the swim bladder corresponding to different numbers of actuated pouches was measured using a customized force sensor. The three inflated configurations of the proposed soft swim bladder were achieved by selectively Joule heating one, two, and three pouches, respectively, as shown in Figure 4A. To test the generated buoyancy force of the soft swim bladder depending on the number of actuated pouches, a pulley was fixed at the bottom of the water container that was connected to the swim bladder and the load cell above the water surface by a cable. This setup allowed unconfined vertical movement of the swim bladder, which allowed for an accurate measure of the generated buoyancy. A float was also attached to the top of the swim bladder to negate the influence of gravity on its weight: the initial buoyancy is zero when no pouches are activated. This experiment was conducted for each number of working pouches from one to three. The force sensor readings were delivered to the Arduino UNO, and the values were averaged to derive the final generated buoyancy force for each number of actuated pouches.

Analysis of the dynamic properties of the swim bladder

A similar set up to the buoyancy force experiment was used without the load cell to analyze the average speed and acceleration of the swim bladder under different circumstances. The movement of the swim bladder for each number of actuated pouches was recorded using a digital camera. Then the displacement, velocity, and acceleration of the pouch, the swim bladder, and the fish robot were measured with Tracker video analysis software (version 5.1.5).

Fish robot test

Optimization of the fishtail

The frequency and amplitude of the fishtail actuation were optimized to yield the best dynamic performance of the fish robot. The actuation cycle is composed of alternate actuation of the tail to each side with an intermediate interval resulting in forward propulsion of the fish robot by moving its tail back and forth. In this experiment, the current amplitude, duration of the actuating signal, and the interval period were varied to determine the optimal actuation cycle. All instances were filmed through a digital camera which was later analyzed to calculate the corresponding speed. The value of the electric current to actuate each SMA wire embedded in the caudal fin was determined to be 0.7A, which was obtained through trial-and-error to allow for full and sustained actuation of the SMA wire. To enable the caudal fin to propel the fish robot forwards smoothly, the actuation cycle of the fishtail was experimentally determined as alternately actuating each SMA wire for 0.6 s with an intermediate interval of 0.2 s. That is, the actuation frequency of the tail was fixed at 0.625 Hz for all follow-up experiments. This configuration resulted in a forward swimming speed of approximately 28.8 mm/s.

Dynamic properties of the fish robot

The fish robot with its main components and dimensions are shown in Figure S5. The dynamic properties were tested in a water tank. This set of experiments for analyzing the robot was conducted in a similar process to the swim bladder by video recording and using video analysis software to calculate its dynamic properties. These videos in Supplementary Information were later edited using video recording software

(Camtasia 9, TechSmith Corp.) to enhance the viewing. First, the depth control function was analyzed according to the number of working pouches without actuating the tail. Since neutral buoyancy was achieved at a single pouch expanded state, heating one and two pouches resulted in the rising and fast-rising modes, respectively, while turning off all pouches resulted in the sinking motion of the fish (Movie S1). The calculated speed and acceleration were based on a fixed distance of 30 cm from its initial position. Movie S2 presents the two motions of rising (rise and fast-rise) and swimming of the fish by actuating the swim bladder to achieve rising and then maintaining neutral buoyancy followed by tail actuation. The swimming-sinking motion was also analyzed in Movie S3. This was done by reversing the order of actuation in the previous example. Next, diagonal-rising, through simultaneous actuation of the tail and swim bladder (Movie S4) for both cases of rising (rise and fast-rise) was analyzed. Lastly, diagonal-sinking was achieved by powering off the swim bladder and actuating the tail at mid-water (Movie S5).

Control unit

The assembled fish robot contains five actuators to be controlled including three pouches in the swim bladder and two SMA wires in the tail actuator. The control unit was accomplished using an Arduino UNO microcontroller with a peripheral circuit including five transistors. The microcontroller utilized both the switching and amplifying properties of the transistor to provide the desired magnitude of current flow at the desired timing. As a result, an overall control architecture capable of controlling each of the segments independently was constructed.

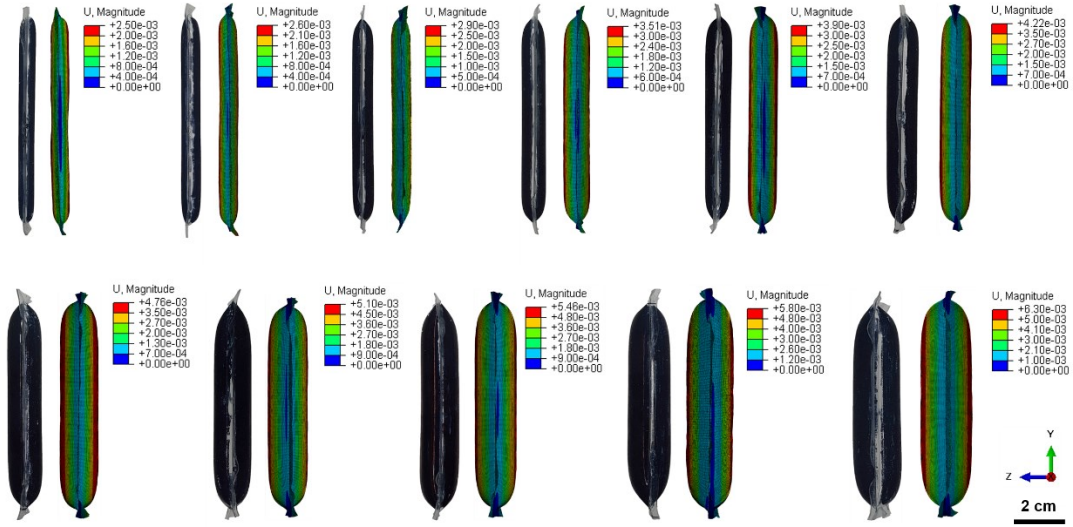


Figure S1. Experimental and modeling results of fully expanded pouches with different widths. The length of the pouch was fixed at 30 mm, and the width was varied from 5 mm to 15 mm, in 1 mm increments.

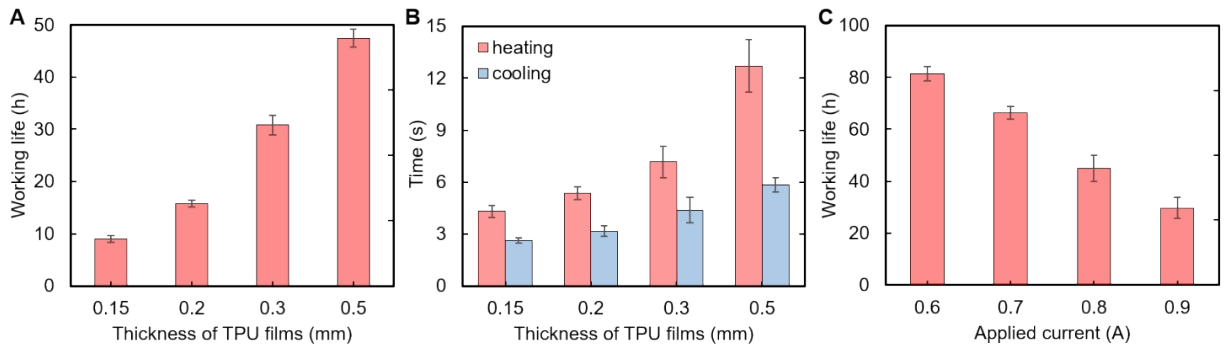


Figure S2. (A) The measurement of the working life of the pouch for different thicknesses of the TPU film with a continuously applied current of 0.8 A. (B) The heating and cooling times required to fully expand and contract the pouch for different thickness of the TPU film underwater at 21 °C. (C) The working life of the pouch with the thickness of the TPU of 0.15 mm for the customized current cycle. Each cycle includes 3.5 s of heating and 3 s of cooling.

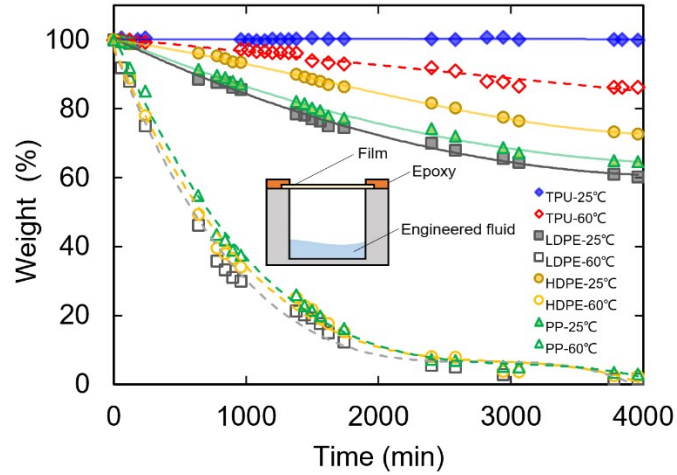


Figure S3. Weight loss test to examine the effects of penetration on the commercially used sealable plastic film at room temperature and 60 °C.

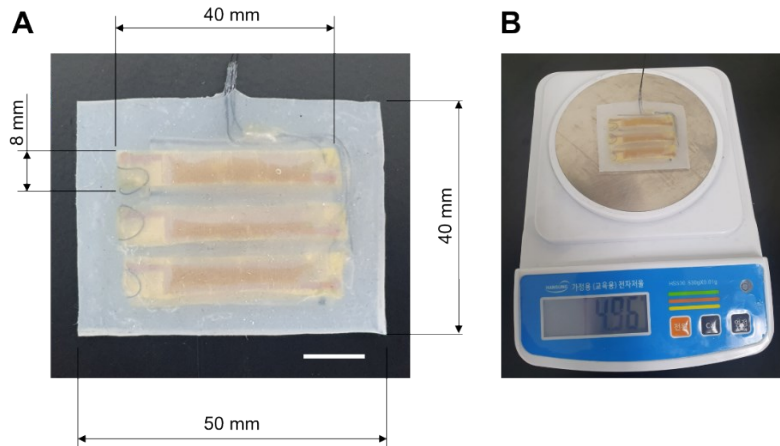


Figure S4. Fabricated swim bladder with its dimensions and weight. (A) Dimensions of the soft swim bladder and buoyancy pouch set, and (B) weight of the soft swim bladder.

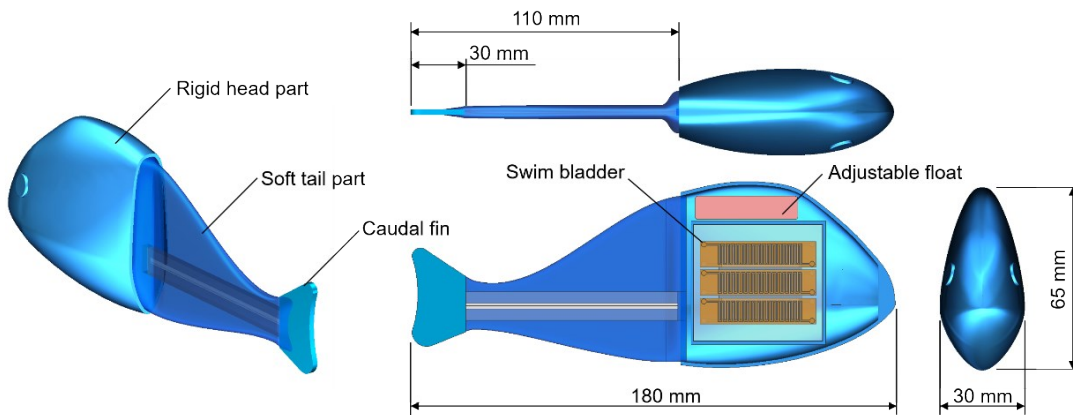


Figure S5. Fabricated fish robot with its dimensions and components. The fish robot mainly consists of a rigid head part including the swim bladder and an adjustable float, and a soft tail part including an SMA-based actuator with a caudal fin.

Table S1. Material properties of the engineered fluid.

| Parameters | Engineered fluid |
|------------------------------------|------------------|
| Liquid density (g/ml) | 1.6 |
| Vapor density (kg/m ³) | 13.73 |
| Volume expansion factor * | 116.5 |
| Boiling points (°C) | 49 |
| Molecular weight (g/mol) | 316 |

*where $\rho_{solution_v}$ is the vapor density of the engineered fluid, and ρ_{air} is the density of the air. Therefore, the volume expansion factor of the engineered fluid with the same weight can be estimated from the following equation:

$$\alpha_{solution} = \rho_{solution_l} / \rho_{solution_v}$$

where $\alpha_{solution}$ is the volume expansion factor of the engineered fluid, and $\rho_{solution_l}$ is the liquid density of the engineered fluid.

Movie S1. Rising and sinking motion of the fish robot.

The rising, fast-rising, and sinking motions of the fish robot depending on the number of buoyancy pouches working are demonstrated, resulting in a speed of 20 mm/s, 40 mm/s, and 19.7 mm/s, respectively.

Movie S2. Rising and swimming motion of the fish robot.

The two motions of rising (rise and fast-rise) and swimming of the fish robot were analyzed. The fish robot raised vertically when two or three pouches were actuated and suspended its position when one pouch was working. Then, forward swimming was achieved through tail actuation while maintaining its depth.

Movie S3. Swimming and sinking motion of the fish robot.

The two motions of swimming and sinking of the fish robot were analyzed. First, the fish robot swam forward by actuating the soft tail while maintaining its depth. Then the fish robot sank without any buoyancy pouch in action.

Movie S4. Diagonal rising motion of the fish robot.

The diagonal-rising motion of the fish robot was demonstrated through simultaneous actuation of the tail and swim bladder.

Movie S5. Diagonal rising motion of the fish robot.

The diagonal-sinking motion of the fish robot was achieved through simultaneous actuation of the tail and swim bladder.